Proceedings of ISFOG 2025
5TH INTERNATIONAL SYMPOSIUM ON
FRONTIERS IN OFFSHORE GEOTECHNICS
Nantes, France | June 9-13 2025

ISBN 978-2-85782-758-0

A Novel Driveability Prediction Method for Continuous Impact Driving and Monopile Run

Shihong Zhang
Zhejiang University, Hangzhou, China

Lizhong Wang, Mengtao Xu, Zhen Guo*

Zhejiang University, Hangzhou, China

Kanmin Shen
PowerChina Huadong Engineering Corporation Limited, Hangzhou, China

Shengjie Rui
Norwegian Geotechnical Institute, Oslo, Norway

* *nehzoug@163.com (corresponding author)*

ABSTRACT: A suitable driveability analysis offers valuable guidance for the construction of pile foundations. This paper proposes a novel driveability prediction method for continuous impact pile driving and monopile run. Both tip gap and cyclic degradation of soil are considered, and the multiple-blow analysis shows that the method can produce accurate predictions of blow counts. Finally, a case of monopile installation in South China Sea is studied, where the behaviour of pile run is captured using the proposed method.

Keywords: Pile driving; Driveability analysis; Cyclic degradation; Pile run

1 INTRODUCTION

Driveability analysis is a critical step before piling, which is conducted to provide an important reference on pile design, hammer selection and the control of impact energy (Buckley et al., 2021). Engineering accidents such as pile run, fatigue damage and tip buckling may occur in the process of impact pile driving, and rational driveability analysis can also help prevent them from happening, ensuring safety and economy (Kourelis et al., 2022; Yenigul et al., 2023). However, traditional driveability analysis is discontinuous due to a limited number of pre-set calculation depths, which induce uncertain errors. Cyclic effects on soil degradation are also not considered.

In this paper, a novel driveability prediction method is proposed to account for the continuous impact driving process. The theoretical framework including the lumped mass-spring system and cyclic soil reaction model are described, followed by the procedure for a specific engineering problem. Multiple-blow driveability analysis and the prediction of monopile run based on the proposed method are then conducted with the comparison to field data.

2 THEORETICAL FRAMEWORK

2.1 Simulation of Continuous Impact Driving

The lumped mass-spring system (see Figure 1) is utilized to simulate the impact process, which is initially proposed by Smith (1960). The ram segment descends from a specified height and strikes the pile cap or the first pile segment. Kinetic energy is transferred, and all lumped masses adhere to Newton's second law. Specifically, each lumped mass is subjected to the internal forces of the pile and the soil resistance. The former are generated by the displacement difference between the lumped mass and the masses above and below it.

To capture the penetration performance under continuous blows, the impact is initiated as soon as the pile displacement stabilizes, slightly increasing the impact frequency due to the ignored time between blows. However, the minimal change in soil properties during this time justifies the simplification. Furthermore, the gap below the pile base will appear when the base spring is subjected to tension but the base segment is still moving upward.

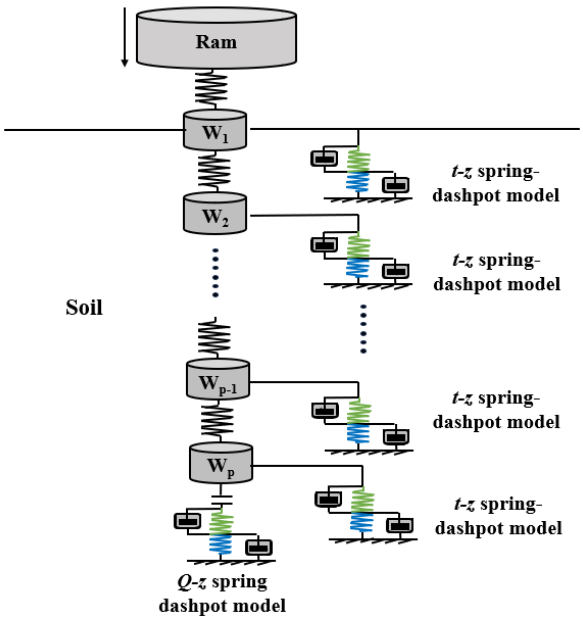

Figure 1 – Lumped mass-spring system for pile driveability analysis.

2.2 Soil Reaction Model Considering Cyclic and Dynamic Effect

To describe the soil behaviour around the pile, the elastoplastic spring-double dashpot model (EPSDD) model is defined (Zhang et al., 2025). The total resistance R_{total} consists of three components as follows:

$$R_{total} = R_{ep} + R_{rad} + R_{vis} \quad (1)$$

where R_{ep} represents the static resistance, and R_{rad} and R_{vis} denote the radiation and viscous damping forces, respectively. As illustrated in Figure 2, the radiation dashpot is connected in parallel with the elastic component of the elastoplastic spring, accounting for energy dissipation due to the propagation of stress waves (Simons, 1985; Lee et al., 1988; Gazetas and Dobry, 1984; Dobry, 2013). The viscous dashpot, which represents strength enhancement due to high strain rates, is positioned in parallel with the plastic spring, rather than with the plastic slider as in traditional models (Simons, 1985; Randolph and Simons, 1986; Randolph, 2003).

The EPSDD model exhibits similar forms in both the shaft and base of the pile. For static resistance, the elastic and plastic components in the elastoplastic spring are arranged in series, with the overall stifffness defined by the form of harmonic mean. According to mapping rule in bounding surface elastoplastic theory (Dafalias and Popov, 1975; Dafalias and Popov, 1976), the plastic stiffness K_p can be calculated as (Zhou et al., 2021):

$$K_p = hK_p[\frac{g(z_p)\cdot r_{u0}}{r_m}\cdot\frac{\bar{\rho}}{\rho} - 1] \quad (2)$$

where h is the shape parameter, $\bar{\rho}$ is the distance of two bounding value, and ρ represents the back projector distance of current stress status. r_{u0} denotes the initial ultimate shear strength t_{u0} in the t-z model and the ultimate base stress q_{u0} in the Q-z model, while r_m is the corresponding maximum stress during loading history. $g(z_p)$ is the degradation function related to the plastic displacement z_p. For damping force, the linear form is used for the radiation dashpot, with the power law applied to the viscous component (Simons. 1985; Coyle and Gibson, 1970; Heerema, 1979; Lysmer and Richart, 1966):

$$r_{rad} = c_{rad}\dot{z}_e \quad (3)$$

$$r_{vis} = r_{ep}\cdot\alpha(\frac{\dot{z}_p}{\dot{z}_{p0}})^{\beta} \quad (4)$$

where r_{rad} and r_{vis} are the unit radiation and viscous damping force. c_{rad} is the radiation damping constant, while α and β are two viscous damping constants. $\dot{z}_e$ and $\dot{z}_p$ represent the displacement rates of the elastic and plastic springs, respectively, with $\dot{z}_{p0}$ denoting the reference value of $\dot{z}_p$, typically taken as 1 m/s (Randolph, 1991).

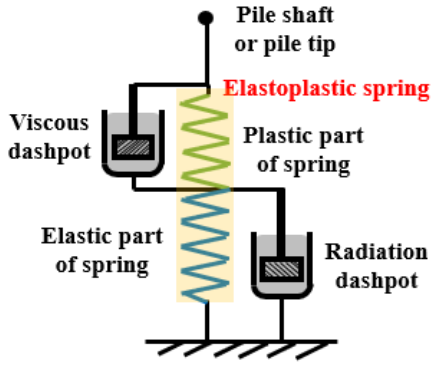

Figure 2 – Elastoplastic Spring-Double Dashpot Soil Reaction Model for continuous impact driving.

Specifically, the calculation methods of para-meters are different in t-z and Q-z models. As shown in Table 1, most parameters are related to basic soil properties, including the small strain shear modulus (G_{max}), and the saturated density (ρ). The elastic stiffness and degradation function of the t-z model can be calibrated primarily through interface shear tests, where z_{50} is the shear displacement corresponding to half of t_{u0}, t_r denotes the residual shear strength, and a and b are degradation constants. L_u, typically taken as 1 m, is the reference displacement. Furthermore, the added mass is incorporated into the Q-z model as proposed by Wolf (1989), which is linked to the pile diameter D, the density ρ and the Poisson ratio v of soil. The dimensionless coefficient α_0 can be set at 0.16 for saturated soil (Deeks and Randolph, 1995).

Table 1. Different formulas of EPSDD parameters for pile shaft and base.

Parameters	*t-z* model	*Q-z* model	Reference
Elastic stiffness K_e	$\frac{t_{u0}}{2z_{50}}$	$\frac{8G_{max}}{(1-\nu)\pi D}$	Zhou et al., 2019; Lysmer and Richart, 1966
Degradation function $g(z_p)$	$\max\left\{\left[(1+\frac{\int\lvert dz_p\rvert}{z_{50}})^{-a}-b\cdot\frac{\int\lvert dz_p\rvert}{L_u}\right],\frac{t_r}{t_{u0}}\right\}$	1	Zhou et al., 2019
Radiation damping constant c_{rad}	$\sqrt{G_{max}\rho}$	$\frac{3.4\sqrt{G_{max}\rho}}{(1-\nu)\pi}$	Simons, 1985; Lysmer and Richart, 1966
Added mass m_a	0	$\frac{\alpha_0\rho D^3}{2(1-\nu)}$	Deeks and Randolph, 1995

2.3 Procedure

For a specific engineering problem, the analysis procedure below is suggested:

(1) Calibrate the pile-soil interface parameters through monotonic and cyclic interface shear tests, and determine fundamental soil parameters, such as G_{max}, using laboratory geotechnical tests like bending beam tests or in-situ CPT tests.
(2) Discretize the pile foundation, establish the lumped mass-spring system and EPSDD soil reaction model integrating the hammer parameters and the calibrated soil parameters.
(3) Establish the mapping relationship of pile and soil at the calculation depth, followed by the initiation of iterative computations, resulting in the generation of displacement-time and cumulative displacement-blow count curve curves.

3 MULTIPLE-BLOW DRIVEABILITY ANALYSIS BASED ON PROPOSED METHOD

Jardine et al. (2006) reports on a field test involving six piles (R1 to R6) driven into dense sand. The blow count is recorded and shows differences under the potential effects of spatial variations in soil properties. Based on the proposed method, the blow counts of R2 to R6 are predicted for depths between 10.5 m and 11.5 m.

In this case, each pile has a length of 19 meters and an outer diameter of 457 mm. The hammer and helmet weigh 4.7 tons. Detailed information regarding the hammer, piles, and soil conditions can be found in Jardine et al. (2006).

For *t-z* spring, the static parameters at Dunkirk have been calibrated by Zhou et al. (2019), with z_{50} set at 0.5 mm and t_r specified as $0.317t_{u0}$. The shaft shape parameter h_s, the degradation constants a and b are set at 4, 0.027, 0.496, respectively. For *Q-z* spring, the base shape parameter h_b is estimated as 0.6 based on Xu et al. (2024). Additionally, the ratio of unloading stiffness to elastic stiffness of shaft friction A_u satisfies the Masing rule (Segalman and Starr, 2008), while for the base stress, it is revised as 3.5 from Achmus et al. (2019). For dynamic parameters, the radiation damping constants are calculated according to Table 1, and viscous damping constants are estimated as 0.3 and 0.2 (Randolph, 2003; Salgado, 2015).

To calculate the soil plug resistance, the linear Smith model (Smith, 1960) is linked to the base segment, while pile R1 is selected to calibrated the soil plug capacity according to Yu and Yang (2012). In the elastic stage, the static plug resistance ($q_{plug,s}$) changes linearly with the spring compression. Once it reaches the plastic stage, the static plug resistance remains constant. In addition to the static plug resistance, the total plug resistance ($q_{plug,tot}$), which can be calculated using the equation (5), also includes a dynamic component.

$$q_{plug,tot} = q_{plug,s}(1 + c\dot{z}) \quad (5)$$

where c is the damping constant, $\dot{z}$ is the displacement rate.

The piles are initially set at the embedment depth of 10.5 m, and the previous penetration process is implicitly considered with the degraded shaft strength estimated by Alm and Hamre (2001). As depicted in Table. 2, the predicted blow counts closely correspond to the recorded values, with all relative errors confined to within 4%.

Table 2. Comparison of predicted blow counts with recorded values.

Pile number	Recorded blow counts	Predicted blow counts	Relative error
R2	158	154	2.5%
R3	195	189	3.1%
R4	246	245	0.4%
R5	208	216	3.8%
R6	186	184	1.1%

4 APPLICATION IN MONOPILE RUN PREDICTION

In this section, a case of monopile run in South China Sea is studied and the proposed method is further applied to predict the process.

As shown in Figure 3, CPTU test and the borehole log demonstrate an alternating distribution of cohesive and sandy soil layers. The monopile measures 81.5 meters in length with a maximum outer diameter of 7.5 meters, which was driven using were driven using IHC-S3000 hammer. The hammer energy is 322 kJ per blow, which remains constant with depth. A pile run distance of 5.75 meters was recorded.

The main input parameters of EPSDD model are listed in Table 3, where the viscous damping constants are evaluated according to Lee (1988) and Heerema (1981). It should be noted that for cohesive soil, the degradation function in *t*-*z* model takes the following form (Yu et al., 2023):

$$g(z_p) = max\left\{\left[\frac{t_r}{t_{u0}} + (1-\frac{t_r}{t_{u0}})e^{-a\cdot\frac{\int|dz_p|}{100z_{50}}}\right], \frac{t_r}{t_{u0}}\right\} \quad (6)$$

K_e, z_{50} and h of cohesive soil are calibrated by Taha and Fall (2014). Furthermore, the ultimate base stress is calculated by $k_q q_{t,a}$ (Bustamante and Gianeselli, 1982), while in this study, the bearing capacity factor k_q also includes the increase of internal friction at the pile tip when penetrating in stiff soil. Two monopiles at the same site are utilized to calibrated the bearing capacity factor at medium dense sand ($k_{q\text{-}MD}$), dense sand ($k_{q\text{-}D}$), and low-plasticity (silty) clay mixed with sand ($k_{q\text{-}LC}$). To consider the layered effects, the changing depth of k_q is modified by CPT-based method of soil classification (Robertson, 1990), while for the excessively thin layer with a thickness less than the diameter of influence zone around the pile base (Yu and Yang, 2012), the value of k_q is assigned equal to that of the adjacent thicker layer.

Different from the case in Section 3, the plug resistance is not represented by a separate soil plug spring, but is incorporated into the *Q*-*z* spring through k_q to improve computational efficiency. To further clarify the composition of the base capacity, the annulus capacity, plug capacity, and total base capacity are calculated separately for both cases, as shown in Figure 4.

To simulate the large-distance penetration behaviour, the mapping relationship between pile and soil is revised to update at each time step according to the real-time position. As illustrated in Figure 4, the predicted cumulative blow counts are closed to the recorded values, and the process of monopile run is successfully captured. The predicted distance of pile run, where the cumulative blow counts no longer increase, is 5.9 m, with a relative error of 2.6%. A limitation is that the blow counts is slightly overpredicted at the low-plasticity silty clay mixed with sand, which may be due to the degradation of base resistance under a high number of cyclic hammer loads.

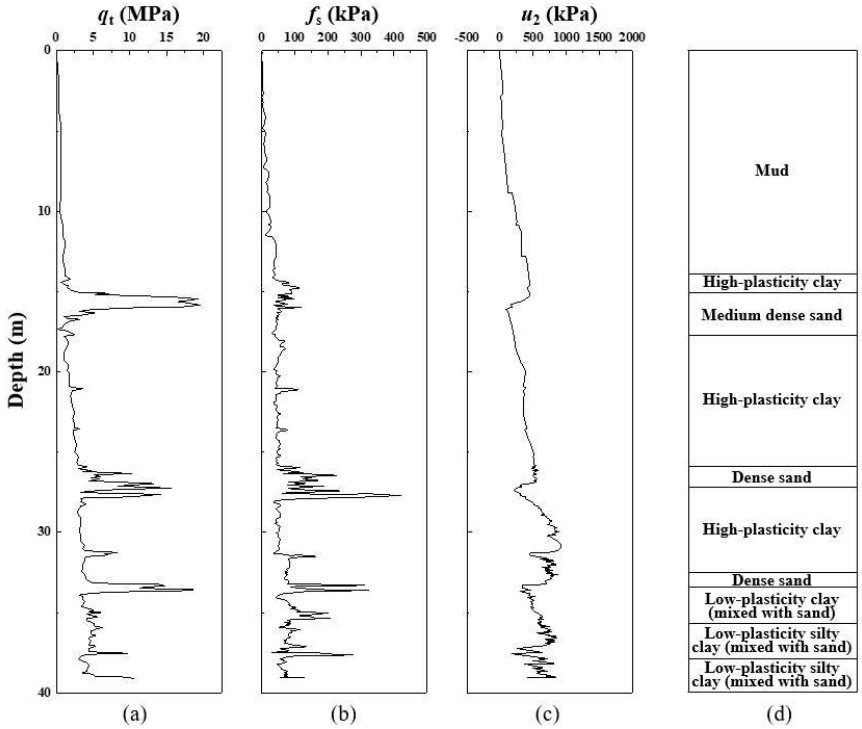

Figure 3 – Profiles of (a) cone resistance, q_t; (b) sleeve friction, f_s; (c) pore pressure, u_2; and (d) borehole log at the site of pile run.

Table 3. Soil parameters for each stratigraphic layer.

Soil description	ρ (kg/m^3)	a, b	h_s	h_b	A_{us}	A_{ub}	α_s, β_s	α_b, β_b
Mud	1666	0.016, 0	0.8	1	2.5	3.5	1.581, 0.2	1.143, 0.2
High-plasticity clay	1923	0.016, 0	0.8	1	2.5	3.5	1.382, 0.2	0.975, 0.2
Medium dense sand	2000	0.001, 2	4	1	2.5	3.5	0, 0.2	2, 0.2
High-plasticity clay	1797	0.016, 0	0.8	1	2.5	3.5	1.279, 0.2	0.887, 0.2
Dense sand	2000	0.0006, 1.9	4	1	2.5	3.5	0, 0.2	2, 0.2
High-plasticity clay	1797	0.016, 0	0.8	1	2.5	3.5	1.246, 0.2	0.859, 0.2
Dense sand	1950	0.0006, 1.9	4	1	2.5	3.5	0, 0.2	0.1, 0.2
Low-plasticity clay (mixed with sand)	1875	0.016, 0	0.8	1	2.5	3.5	1.173, 0.2	0.797, 0.2
Low-plasticity silty clay (mixed with sand)	1875	0.016, 0	0.8	1	2.5	3.5	1.173, 0.2	0.797, 0.2
Low-plasticity silty clay (mixed with sand)	1949	0.016, 0	0.8	1	2.5	3.5	1.068, 0.2	0.708, 0.2

* The subscripts *s* and *b* denote that the parameter is used for the *t-z* and *Q-z* models, respectively.

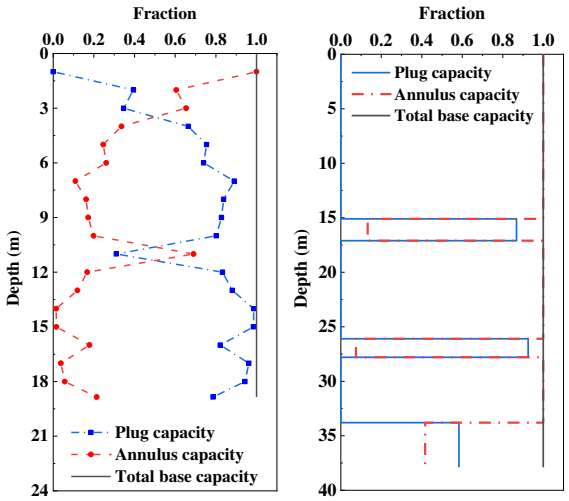

Figure 4 – Proportion of plug capacity and annulus capacity in total base capacity: (a) Pile R1 in Dunkirk site; (b) Monopile in South China Sea.

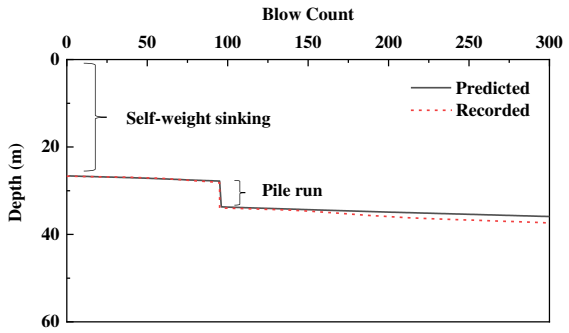

Figure 5 – Comparison of predicted cumulative blow counts with recorded values.

5 CONCLUSIONS

A novel method for predicting driveability is proposed, enabling continuous analysis of cyclic impact driving. The theoretical framework is outlined, accompanied by a description of the recommended procedure. Two practical case studies are also presented. The primary conclusions are:

(1) In the proposed method, the lumped mass-spring system is adjusted to simulate the continuous driving process with the effect of tip gap, while the elastoplastic spring is incorporated into the soil reaction model with cyclic shaft degradation expressed as the function of cumulative plastic displacement.

(2) Both onshore and offshore cases demonstrate the effectiveness of the proposed method in predicting blow counts and pile run. The errors are within acceptable limits, and future research should focus on the potential variation in base resistance under a large number of cyclic hammer loads.

AUTHOR CONTRIBUTION STATEMENT

Shihong Zhang: Writing - original draft, Visualization, Validation, Software, Methodology. **Lizhong Wang**: Conceptualization, Methodology, Project administration. **Mengtao Xu**: Validation, Visualization, Investigation. **Kanmin Shen**: Visualization, Investigation. **Shengjie Rui**: Visualization, Validation. **Zhen Guo:** Conceptualization, Investigation, Supervision, Writing-Reviewing and Editing.

ACKNOWLEDGEMENTS

The authors would like to acknowledge the supports from the National Key R&D Program of China (2023YFB4203301, 2023YFB4203303), National Natural Science Foundation of China (52238008, 52101334), Natural Science Foundation of Zhejiang Province (LR22E080005).

REFERENCES

Achmus, M., Thieken, K., Saathoff, J. E., Terceros, M., and Albiker, J. (2019). Un-and reloading stiff-ness of monopile foundations in sand. *Applied Ocean Research*, 84: 62-73. https://doi.org/10.1016/j.apor.2019.01.001

Buckley, R. M., Kontoe, S., Jardine, R. J., Barbosa, P.,and Schroeder, F. C., 2021. Pile driveability in low-to medium-density chalk. Canadian Geotechnical Journal, 58(5): 650-665. https://doi.org/10.1139/cgj-2019-0703

Bustamante, M., and Gianeselli, L. (1982). Pile bearing capacity prediction by means of static penetrometer CPT. In: *Proceedings of the 2nd European symposium on penetration testing*, Balkema, Amsterdam, the Netherlands, Vol. 2, pp. 493-500.

Coyle, H. M., and Gibson, G. C. (1970). Empirical damping constants for sands and clays. *Journal of the Soil Mechanics and Foundations Division*, 96(3): 949-965. https://doi.org/10.1061/JSFEAQ.0001427

Dafalias, Y. F., and Popov, E. P. (1975). A model of nonlinearly hardening materials for complex loading. *Acta mechanica*, 21(3): 173-192. https://doi.org/10.1007/BF01181053

Dafalias, Y. F., and Popov, E. P. (1976). Plastic Internal Variables Formalism of Cyclic Plasticity. *ASME Journal of Applied Mechanics*, 43: 645-651. https://doi.org/10.1115/1.3423948

Deeks, A. J., and Randolph, M. F. (1995). A simple model for inelastic footing response to transient loading. *International journal for numerical and analytical methods in geomechanics*, 19(5): 307-329. https://doi.org/10.1002/nag.1610190502

Dobry, R. (2013). Radiation damping in the context of one-dimensional wave propagation: A teaching perspective. *Soil Dynamics and Earthquake Engineering*, 47: 51-61. https://doi.org/10.1016/j.soildyn.2012.08.014

Gazetas, G., and Dobry, R. (1984). Simple radiation damping model for piles and footings. *Journal of Engineering Mechanics*, 110(6): 937-956. https://doi.org/10.1061/(ASCE)0733-9399(1984)110:6(937)

Heerema, E. P. (1979). Relationships between wall friction, displacement velocity and horizontal stress in clay and in sand, for pile driveability analysis. *Ground engineering*, 12(1): 55-60.

Heerema, E. P. (1981). Dynamic point resistance in sand and in clay, for pile driveability analysis. *Ground Engineering*, 14(6): 30-46.

Jardine, R. J., Standing, J. R., and Chow, F. C. (2006). Some observations of the effects of time on the capacity of piles driven in sand. *Géotechnique*, 56(4): 227-244. https://doi.org/10.1680/geot.2006.56.4.227

Kourelis, I., Kontoe, S., Buckley, R., and Galbraith, A. (2022). An assessment of pile driveability analyses for monopile foundations. In: *International Conference on Stress Wave Theory and Design and Testing Methods for Deep Foundations*, Rotterdam, The Netherlands.

Lee, S. L., Chow, Y. K., Karunaratne, G. P., and Wong, K. Y. (1988). Rational wave equation model for pile-driving analysis. *Journal of Geotechnical Engineering*, 114(3): 306-325. https://doi.org/10.1061/(ASCE)0733-9410(1988)114:3(306)

Lysmer, J. F. E. R., and Richart Jr, F. E. (1966). Dynamic response of footings to vertical loading. *Journal of the Soil Mechanics and Foundations Division*, 92(1): 65-91. https://doi.org/10.1061/JSFEAQ.0000846

Randolph, M. F., and Simons, H. A. (1986). An improved soil model for one dimensional pile driving analysis. In: *Third International Conference on Numerical Methods in Offshore Piling*, Nantes, France, pp. 3-17.

Randolph M F. (1991). *Developments in Soil Mechanics IV: Advanced Geotethoical Analyses*, 1st ed., Elsevier Applied Science Publishers Ltd. London.

Randolph, M. F. (2003). Science and empiricism in pile foundation design. *Géotechnique*, 53(10): 847-875. https://doi.org/10.1680/geot.2003.53.10.847

Robertson, P. K. (1990). Soil classification using the cone penetration test. *Canadian geotechnical journal*, 27(1): 151-158. https://doi.org/10.1139/t90-014

Segalman, D. J., and Starr, M. J. (2008). Inversion of Masing models via continuous Iwan systems. *International Journal of Non-Linear Mechanics*, 43(1): 74-80. https://doi.org/10.1016/j.ijnonlinmec.2007.10.005

Simons, H. A. (1985). *A theoretical study of pile driving*. PhD thesis, University of Cambridge.

Smith, E. A. L. (1960). Pile-driving analysis by the wave equation. *Journal of the soil mechanics and foundations division*, 86(4): 35-61. https://doi.org/10.1061/JSFEAQ.0000281

Taha, A., and Fall, M. (2014). Shear behavior of sensitive marine clay–steel interfaces. *Acta Geotechnica*, 9: 969-980. https://doi.org/10.1007/s11440-014-0321-4

Wolf, J. P. (1989). Soil-structure-interaction analysis in time domain. *Nuclear engineering and design*, 111(3): 381-393. https://doi.org/10.1016/0029-5493(89)90249-5

Xu, M., Wang, L., Wang, L., Guo, Z., and Zhou, W. (2024). Influence of bounding surface plasticity-

based soil-structure interaction model on integrated dynamic behaviour of jacket offshore wind turbines. *Ocean Engineering*, 298, 117204. https://doi.org/10.1016/j.oceaneng.2024.117204

Yenigul, N. B., Yan, Y., Braakenburg, L. C. H., and Thumann, V. M. (2023). Evaluation of pile driveability predictions in sand. In: *Offshore Site Investigation Geotechnics 9th International Conference Proceeding*, London, UK, Vol. 758, No. 763, pp. 758-763.

Yu, F., and Yang, J. (2012). Base capacity of open-ended steel pipe piles in sand. *Journal of Geotechnical and Geoenvironmental Engineering*, 138(9): 1116-1128. https://doi.org/10.1061/(ASCE)GT.1943-5606.0000667

Yu, S. W., Wang, J., Liu, J. W., and Wang, T. (2023). Experimental studies on cyclic shear behavior of steel-clay interface under constant normal load. *China Ocean Engineering*, 37(3): 519-524. https://doi.org/10.1007/s13344-023-0043-1

Zhang, S., Wang, L., Xu, M., Rui, S., Guo, Z. (2025) A novel soil reaction model for continuous impact pile driving. Computers and Geotechnics, 181, 107123. https://doi.org/10.1016/j.compgeo.2025.107123

Zhou, W., Wang, L., Guo, Z., Liu, J., and Rui, S. (2019). A novel tz model to predict the pile responses under axial cyclic loadings. *Computers and Geotechnics*, 112: 120-134. https://doi.org/10.1016/j.compgeo.2019.04.027

Zhou, W., Guo, Z., Wang, L., Zhang, Y., and Rui, S. (2021). Numerical model for suction caisson under axial cyclic loadings. *Ocean Engineering*, 240: 109956. https://doi.org/10.1016/j.oceaneng.2021.109956